

Intraoperative delineation of primary brain tumors using time-resolved fluorescence spectroscopy

Pramod V. Butte

Cedars-Sinai Medical Center
Department of Neurosurgery
8631 West 3rd Street, Suite 800E
Los Angeles, California 90048
and

University of Southern California
Department of Biomedical Engineering
451 Health Sciences Drive
Los Angeles, California 90007

Qiyin Fang*

Javier A. Jo*

Cedars-Sinai Medical Center
Department of Surgery
8700 Beverly Blvd., 8215 NT
Los Angeles, California 90048

William H. Yong*

University of California, Los Angeles
Department of Pathology and Laboratory Medicine
CHS 18-161
CAMPUS-173216
Los Angeles, California 90095

Brian K. Pikul*

Keith L. Black

Cedars-Sinai Medical Center
Department of Neurosurgery
8631 West 3rd Street, Suite 800E
Los Angeles, California 90048

Laura Marcu

University of Southern California
Department of Biomedical Engineering
451 Health Sciences Drive
Los Angeles, California 90007
and

University of California, Davis
Biomedical Engineering
Genome Biomedical Science Facility
451 Health Sciences Drive, Room 2513
Davis, California 95616

1 Introduction

Gliomas represent 40% of all primary brain tumors, and treatment of glioma poses a challenge due to their tendency to infiltrate the surrounding normal brain. Astrocytoma and glioblastoma are the two most common types of gliomas. The

Abstract. The goal of this study is to determine the potential of time-resolved laser-induced fluorescence spectroscopy (TR-LIFS) as an adjunctive tool for delineation of brain tumor from surrounding normal tissue in order to assist the neurosurgeon in near-complete tumor excision. A time-domain TR-LIFS prototype apparatus (gated photomultiplier detection, fast digitizer) was used for recording tissue autofluorescence in normal cortex (NC), normal white matter (NWM), and various grades of gliomas intraoperatively. Tissue fluorescence was induced with a pulsed nitrogen laser (337 nm, 700 ps), and the intensity decay profiles were recorded in the 360- to 550-nm spectral range (10-nm interval). Histopathological analysis (hematoxylin & eosin) of the biopsy samples taken from the site of TR-LIFS measurements was used for validation of spectroscopic results. Preliminary results on 17 patients demonstrate that normal cortex ($N=16$) and normal white matter ($N=3$) show two peaks of fluorescence emission at 390 nm (lifetime= 1.8 ± 0.3 ns) and 460 nm (lifetime= 0.8 ± 0.1 ns). The 390-nm emission peak is absent in low-grade glioma ($N=5$; lifetime= 1.1 ns) and reduced in high-grade glioma ($N=9$; lifetime= 1.7 ± 0.4 ns). The emission characteristics at 460 nm in all tissues correlated with the nicotinamide adenine dinucleotide fluorescence (peak: 440 to 460 nm; lifetime: 0.8 to 1.0 ns). These findings demonstrate the potential of using TR-LIFS as a tool for enhanced delineation of brain tumors during surgery. In addition, this study evaluates similarities and differences between TR-LIFS signatures of brain tumors obtained *in vivo* and those previously reported in *ex vivo* brain tumor specimens. © 2010 Society of Photo-Optical Instrumentation Engineers. [DOI: 10.1117/1.3374049]

Keywords: glioma; time resolved; fluorescence; spectroscopy; intraoperative; autofluorescence.

Paper 09293R received Jul. 16, 2009; revised manuscript received Jan. 18, 2010; accepted for publication Feb. 9, 2010; published online Apr. 14, 2010.

current 18-month survival rate of glioblastoma patients treated with surgery for biopsy only, partial resection, and complete resection is 15%, 25%, and 34% respectively, making it one of the most lethal tumors.¹ The standard treatment for brain tumor patients is surgery followed by radiation or chemotherapy. The extent of surgical resection is a primary determinant of outcome, and it was shown that the extent of tumor resection is a single most important factor for longer survival.^{2,3} The surgical resection is complicated by location of these tumors, as they may be embedded in or near the

*Currently Qiyin Fang is with McMaster University, Hamilton, ON, Javier A. Jo is with Texas A&M University, Bryan, TX, Brian Pikul is with Kaiser Permanente, Los Angeles, CA, and William H. Yong is with University of California, Los Angeles, CA.

Address all correspondence to: Laura Marcu, University of California, Davis, Department of Biomedical Engineering, Genome Biomedical Science Facility, 451 Health Sciences Drive, Room 2513, Davis, California 95616. Tel: 530-752-0288; Fax: 530-754-5739; E-mail: lmarcu@ucdavis.edu

eloquent areas of the brain such as motor cortex, sensory cortex, and speech centers. Determining the functional areas and the resectable tumor during the surgery has presented a great challenge.

In order to overcome such problems, currently several techniques are employed by surgeons in their quest for near complete removal of the tumor. This includes stereotactic image-guided surgery that delineates the tumor and intraoperative ultrasound or electric mapping to determine the functional areas from the tumor. Stereotactic image-guided surgery based on pre operative magnetic resonance imaging (MRI) scans could be used to determine the position of excision with respect to the position of tumor. However, this technique has intrinsic confounding factors such as the brain shift that occurs during the surgery. This shift may be due to loss of cerebral spinal fluid or due to release of pressure; this can result in significant inaccuracies in resection of the tumor. More recently, in order to eliminate these limitations, many major medical centers have employed intraoperative MRI (iMRI). This technique requires, however, a major investment and modification of operating room settings as well as surgical instrumentation. Moreover, the actual pathological diagnosis can be provided only by biopsy and frozen section, which requires 15 to 20 min and can be used only in limited capacity. Even in the hands of the most skilled surgeon, complete excision is limited by the tactile and visual feedback. Thus, in order to enhance the ability of the surgeon to excise completely the tumor with more accuracy without sacrificing safety, new technologies need to be developed. Such new technologies should be able to distinguish accurately between the tumor and normal brain and guide the tumor resection in near-real time.

Laser-induced fluorescence spectroscopy (LIFS) represents a promising new adjunctive technique in the diagnosis of tissue pathologies.⁴⁻⁸ Fluorescence spectroscopy involves the use of lasers to excite endogenous autofluorescence (label-free) within tissues. Either the steady-state^{5,9,10} or the time-resolved^{6,11,12} fluorescence spectroscopy technique can be used to measure or monitor these changes. The time-resolved measurement resolves fluorescence intensity decay in terms of excited-state lifetimes and thus provides additional information about the underlying fluorescence intensity decay dynamics and improves its specificity. Earlier work has demonstrated that label-free steady-state LIFS of endogenous fluorophores (autofluorescence) can be used as a tool for diagnosis of neoplasm in the brain. Several types of brain tumors have been investigated, both *in vivo* and *ex vivo*, using this technique. These include studies of glioblastoma,^{5,6,9} astrocytoma,⁹ oligodendroglioma,⁹ and metastatic carcinoma.⁹ In addition, our group has previously reported results on the utility of time-resolved LIFS (TR-LIFS) for distinguishing glioblastoma from uninvolved cerebral cortex and white matter and on its increased specificity relative to steady-state fluorescence spectroscopy.^{6,11,12}

The overall objective of this study is to investigate the use of TR-LIFS as a rapid diagnostic tool for intraoperative delineation of tumor from surrounding normal tissue. Such a tool has a potential to enhance the ability of the neurosurgeon-neuropathologist to distinguish between tumor and normal brain during surgery. Extending on our earlier work conducted

in *ex vivo* specimens,^{6,12} The current study is designed (1) to determine the spectrum- and time-dependent autofluorescence emission characteristics of gliomas (high- and low-grade), normal cortex (NC), and normal white matter (NWM) measured *in vivo* in patients undergoing surgical resection of brain tumors; and (2) to identify the main autofluorescence signatures that provide means of discrimination between tumor and normal tissue. In addition, this study evaluates the possible differences between fluorescence signatures measured *in vivo* versus those measured *ex vivo* in tumor specimens as reported earlier.^{6,12}

2 Materials and Methods

2.1 Patient/Samples

A total of 17 patients diagnosed with a primary brain tumor (glioma) were included in this study. The patients were scheduled for surgical removal of the brain tumor and underwent the planned operation. During this procedure, the TR-LIFS fiber-optic probe was positioned above the areas of interest using a Greenburg retractor, and the brain tissue was spectroscopically investigated (total: 34 locations). While for this study, we recorded the fluorescence emission for multiple sites ($n=123$), the biopsy was performed at the surgeon's decision based on the suitability of each location for biopsy. Thus, we report here only data from the sites where biopsy was available. Areas with distinct pathologic features were selected based on the gross visual evaluation by the neurosurgeon who-performed the surgery and preoperative MRI scans typically used to guide the surgery. For future validation, intraoperative biopsy was conducted at each point of spectroscopic investigation, except for areas considered normal or not considered suitable for physical biopsy due to risks posed to the patient. The study was carried out with approval of the Cedars-Sinai Medical Center Institutional Review Board.

2.2 Instrumentation

Experiments were conducted with an instrumental setup, which allowed for spectrally resolved fluorescence lifetime measurements. A schematic of the optical and electronic layout of the apparatus is shown in Fig. 1. A detailed account of this apparatus and its performance is given elsewhere.¹³ Briefly, it consisted of (1) a pulsed nitrogen laser (Lasertechnik Berlin, Berlin, Model MNL200-ATM205, $\lambda=337$ nm, pulse width=700 ps FWHM), which was used as the excitation source; (2) a custom-made sterilizable bifurcated fiber-optic probe (CeramOptec, East Longmeadow, Massachusetts); (3) an imaging spectrometer/monochromator (Chromex, Inc., Albuquerque, New Mexico, Model 250is/sm, F/4.4, 600 gr/mm grating, blazed at 450 nm); (4) a gated multi-channel plate photomultiplier tube (MCP-PMT; Hamamatsu, Bridgewater, New Jersey, Model R5916-50, rise time = 180 ps) with a fast preamplifier (Hamamatsu, Bridgewater, New Jersey, Model C5594, 1.5 GHz); (5) a digital phosphor oscilloscope (TDS5104, Tektronix, Beaverton, Oregon, 5 Giga-samples/s); and (6) a computer workstation and peripheral electronics. The instrument allowed for mobility, as it was contained in a standard endoscopic cart ($70 \times 70 \times 150$ cm³), internally modified to accommodate the individual devices.

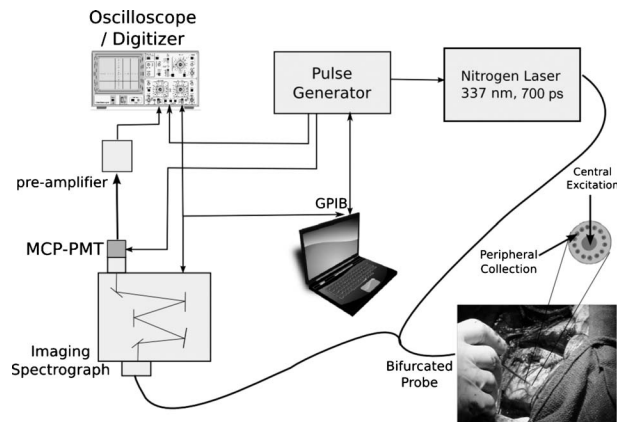


Fig. 1 Schematic of the pulse-sampling TR-LIFS apparatus, including a fast digitizer and gated detection used for the *in vivo* evaluation of brain tumor time-resolved fluorescence emission. Photo shows the tip of the optical probe used on the brain tissue (cortex of a patient undergoing brain tumor surgery).

2.2.1 Delivery catheter

Light delivery and collection were implemented with a custom-made bifurcated sterilizable probe. The probe consisted of nonsolarizing silica/silica step index fibers of 0.11 numerical aperture (NA; CeramOptec, East Longmeadow, Massachusetts). It had a central excitation fiber of 600- μm core diameter, surrounded by a collection ring of twelve 200- μm -core-diameter fibers. The collection fibers were beveled at a 10-deg angle in order to improve excitation/collection overlap for small tissue-to-probe distances. The center-to-center separation between the excitation and collection fibers was 480 μm . The probe was flexible throughout its entire length (3 m) except for a 7-cm distal part consisting of a rigid stainless steel tube. This facilitated the mounting and micromanipulation of the probe. The laser light was coupled into the illumination channel of the probe with a standard subminiature version A (SMA) connector, while the distal end of the collection channel was formed into a straight line in order to facilitate coupling to the spectrograph. After sample excitation, the emitted fluorescence light was collected and directed into the entrance slit of the spectrometer via the col-

lection channel of the probe. A long-pass filter (WB360, Optima, Tokyo, $\lambda=345$ nm) was placed before the entrance slit of the monochromator to prevent contamination of the fluorescence signal by the excitation light. The signal was then detected by the MCP-PMT, amplified by the fast preamplifier, and finally digitized at 8 bits resolution by the digital oscilloscope. The overall time resolution of the systems was approximately 300 ps.

2.3 Experimental Procedure

The fiber-optic probe was positioned at 3 mm above the exposed brain tissue specimen by the Greenburg retractor to optimize the probe light collection efficiency as previously reported¹⁴ and to steady the probe over the tissue. Time-resolved emission of each sample was recorded in the 370- to 550-nm spectral range and scanned at 5-nm intervals (Fig. 2). The total amount of time required to obtain a complete time-resolved spectra by scanning through all the wavelengths is approximately 30 s. Five consecutive measurements of the fluorescence pulse emission at 390 and 460 nm were performed to assess the reproducibility of the fluorescence lifetime measurement. The energy output of the laser (at the tip of the fiber) for sample excitation was adjusted to 3.0 $\mu\text{J}/\text{pulse}$. The area illuminated by the probe (defined by the NA of the excitation fiber and the probe-to-tissue distance) was approximately 2 mm^2 ; thus, the total fluence per pulse at the tissue level was approximately 1.4 $\mu\text{J}/\text{mm}^2$, which is very well within the safety limits. After the spectroscopic analysis, the tissue was biopsied at the exact site and sent for pathological investigation.

2.4 Histopathological Analysis

Except for the normal cortex (NC), tissue was biopsied from the areas where fluorescence was recorded. Each biopsy sample was fixed in 10% buffered formalin. The tissue samples were then cut and fixed on the slides; the slides were stained by the standard hematoxylin & eosin (H&E) stain. All slides were studied by the pathologist and correlated with original fluorescence spectroscopy measurements results. Histologically, gliomas are categorized in low-grade (grade I), intermediate-grades (grades II and III), and high-grade gliomas or glioblastoma multiforme (grade IV), which is based on

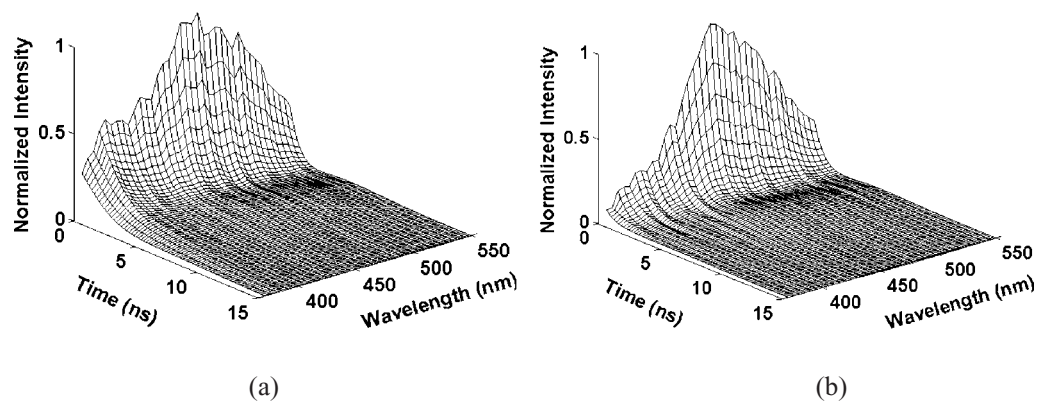


Fig. 2 Typical fluorescence impulse response function (FIRF) from (a) normal cortex and (b) low-grade glioma after deconvolving the laser signal using the Laguerre deconvolution technique.

the WHO grading (Kernohan and Sayred).¹⁵ In the current study, however, we grouped the gliomas in two sets: low-grade glioma (LGG), including grades I and II, and high-grade glioma (HGG), including grades III and IV.

2.5 TR-LIFS Data Analysis

In the context of TR-LIFS, the intrinsic fluorescence impulse response functions (FIRFs), $h(n)$, describe the real dynamics of the fluorescence decay. The IRFs were recovered by numerical deconvolution of the measured input laser pulse from the measured fluorescence response pulse transients. The Laguerre expansion of kernels technique.¹⁶ was used for deconvolution. This method allows a direct recovery of the intrinsic properties of a dynamic system from the experimental input-output data. The technique uses the orthonormal Laguerre functions $b_i^a(n)$ to expand the IRFs and to estimate the Laguerre expansion coefficients (LECs) c_f . Once the fluorescence IRFs were estimated for each emission wavelength, the steady-state spectrum (I_2) was computed by integrating each intensity decay curve as a function of time. Further, to characterize the temporal dynamics of the fluorescence decay, two sets of parameters were used: (1) the average lifetime (τ_f) computed as the interpolated time at which the IRF decays to $1/e$ of its maximum value; and (2) the normalized value of the corresponding LECs. Thus, a complete description of the fluorescence emission from each sample as a function of emission wavelength, λ_E , was given by the variation of a set of spectroscopic parameters (I_λ , τ_f , and LECs). This analytical approach for characterization of fluorescence decay was recently developed by our research group, and its advantages over other deconvolution methods are described in detail elsewhere.^{16,17}

2.6 Statistical Analysis

Parameters derived from the time-resolved fluorescence spectrum were used for the discrimination of distinct types of tissue. These parameters were based on the discrete fluorescence intensity (I_λ), average lifetime (τ_λ), and Laguerre coefficient (LECs) values at all recorded wavelengths. A univariate statistical analysis (one-way ANOVA) was used to identify a set of spectroscopic parameters that best discriminate between distinct tissue types as defined by the histopathologic analysis. This was achieved by comparing time-resolved derived parameters (τ_f and LECs) at every λ_E and intensity ratios (I_r) at discrete wavelengths. A P -value of <0.05 was assumed to indicate statistically significant differences. A systematic comparison of the P -values obtained for each parameter at every λ_E allowed us to identify a set of spectroscopic parameters (I_r , τ_f and LECs at specific λ_E s yielding the lowest P -values) likely to provide means of discrimination among different compositional features of the brain tissue. All statistical analysis was conducted using SPSS (SPSS, Inc., Chicago, Illinois).

3 Results

3.1 Histology

The histological examination revealed the presence of the following tissue types: NC=normal cortex ($N=16$); NWM=normal white matter ($N=3$); LGG=low-grade glioma with

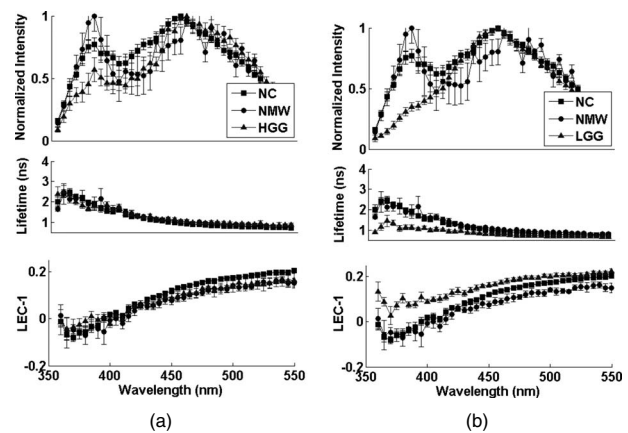


Fig. 3 Fluorescence emission spectra (top), average lifetimes (middle), and Laguerre coefficients (LEC-1) (bottom) across the emission wavelengths for distinct brain tissue types. (a) Normal cortex (NC), normal white matter (NWM), and high-grade glioma (HGG). (b) Normal cortex, normal white matter and low-grade glioma (LGG). Note: The average lifetimes of the LGG is relatively constant across the wavelength compared to the average lifetimes of NC, NWM, and HGG.

WHO grade I or II ($N=5$); and HGG=high-grade glioma with WHO grade III or IV ($N=9$). In addition, the histological analysis revealed that the cells underlying the areas of laser excitation were not visibly altered post-excitation and had a well-preserved morphology.

3.2 Spectroscopic Features

Figure 2 shows the typical fluorescence response IRF from which the fluorescence emission spectra and the average lifetime were recovered. The NC (Fig. 3) autofluorescence was characterized by a broad emission spectrum with two well-defined peaks, one within the 440- to 460-nm wavelength range, and the other at shorter emission wavelengths at approximately 390 nm. The former peak is consistent with the fluorescence emission of enzyme cofactor nicotinamide adenine dinucleotide (NADH). Attenuation of fluorescence intensity was observed at about 415 nm that corresponds to the hemoglobin absorption band. The lifetime (τ_λ) or the intensity decay characteristics (Fig. 3) in the normal cortex showed that the emission was significantly ($p < 0.001$) longer lasting at blue-shifted ($\tau_{390} = 1.8 \pm 0.3$ ns) when compared with the red-shifted ($\tau_{460} = 0.8 \pm 0.1$ ns) wavelengths. The lifetimes observed at 460 nm are consistent also with the NADH lifetime reported in the literature.^{4,18,19} The NWM was characterized by a similar broad fluorescence emission spectrum (Fig. 3) with two well-defined peaks around 390 and 440 nm, the latter corresponding to emission enzyme cofactor NADH, respectively. The attenuation of fluorescence intensity observed at about 415 nm corresponds to the hemoglobin absorption band.¹⁰ The average fluorescence lifetime (Fig. 3) showed similar characteristics as NC with longer lasting emission values in the blue-shifted ($\tau_{390} = 1.9 \pm 0.5$ ns) when compared with the red-shifted ($\tau_{460} = 1.0 \pm 0.04$ ns) wavelengths ($p = 0.02$). The fluorescence emission spectra of LGG samples showed a relatively narrow broadband emission characterized by a single well-defined peak at 460-nm wavelength [Fig.

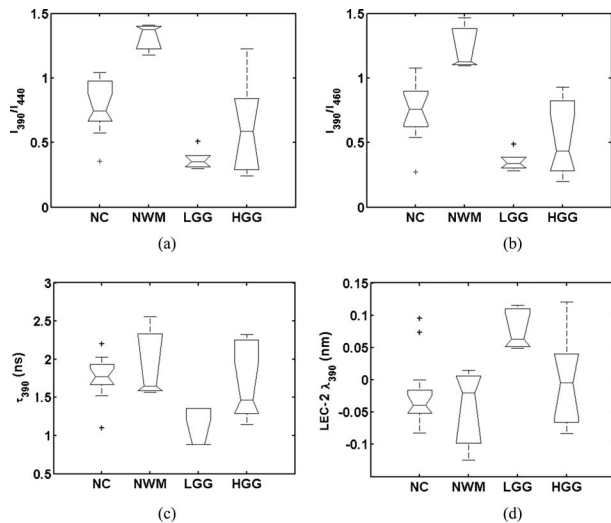


Fig. 4 Representative examples of spectroscopic parameters (mean \pm SE) that allows for the differentiation of distinct tissue types (a) Intensity ratio 390 nm versus 440 nm; (b) intensity ratio 390 versus 460; (c) average lifetime at 390 nm; and (d) Laguerre coefficients at 390 nm. (NC=normal cortex; NWM=normal white matter; HGG=high-grade glioma; LGG=low-Grade glioma.) Note: LGG demonstrates low variance as compared with high-grade glioma and can be readily distinguished from normal brain tissue. On each box, the central mark is the median, the edges of the box are the 25th and 75th percentiles, the whiskers extend to the most extreme data points not considered outliers, and outliers are plotted individually.

3(b)] lasting for less than 1 ns. Across the entire spectrum, the fluorescence emission decay was short-lasting, with an average lifetime mainly at about 1.1 ns. As clearly observed, the LGG shows a very distinct average lifetime when compared with NC ($p=0.0009$), NWM ($p=0.015$), and HGG ($p=0.005$) at 390 nm. HGG demonstrated similar fluorescence emission spectrum to NC with a well-defined peak between 440- to 460-nm wavelengths, which is consistent^{4,18,20} with emission of enzyme cofactor NADH, and a second smaller peak at 390 nm. Similar attenuation of fluorescence intensity at about 415 nm that corresponds to the hemoglobin absorption band was also observed. The fluorescence emission closely followed the trend observed in normal cortex τ_{390} at 1.7 ± 0.4 ns and τ_{460} at $1.0 \text{ nm} \pm 0.9$ ns ($p < .001$).

3.3 Statistical Analysis

The results of the ANOVA demonstrated that the following parameters were within the statistical significance (p -value < 0.01): I_{390}/I_{370} , I_{440}/I_{370} , I_{460}/I_{370} , I_{390}/I_{500} , I_{390}/I_{440} , I_{390}/I_{460} , τ_{390} , τ_{440} , τ_{460} , LEC-1₃₉₀, LEC-1₄₄₀, LEC-1₄₆₀, LEC-2₃₉₀, LEC-2₄₄₀, LEC-2₄₆₀, and LEC-3₃₉₀. This set of parameters including I_r , τ_f , LECs were found able to discriminate between the four type of tissues of interest (LGG, HGG, NC, and NWM). Figure 4 demonstrates the mean with the dispersion and skewness. Spectroscopic parameters derived from both spectral domain (I_r) and time domain (τ_f , LECs) were able to distinguish LGG from healthy brain tissue (NC, NWM). These parameters were generally characterized by a narrow distribution around the mean value. In contrast, the parameters derived for HGG exhibited a broad distribution. A few parameters were able to distinguish HGG tissue from

NWM, but not from NC. Overall, based on this analysis of variance test, we determined that most of the time-resolved fluorescence parameters that help in distinguishing between the four tissue types were derived from three wavelengths: 390 nm, 440 nm, and 460 nm. In addition, intensity ratios including intensity values derived from the main peak emissions (390 nm and 440 to 460 nm) are important for tissue discrimination.

4 Discussion

By examining the *ex vivo* brain tumor tissue using TR-LIFS, we demonstrated previously^{6,12} that this technique has the potential to characterize and diagnose brain tumors. Extending on these early results, in this study, we examined for the first time *in vivo* the fluorescence emission of low- and high-grade gliomas and compare this with that of normal brain tissue. We demonstrated that TR-LIFS could be used to distinguish between the glioma tissue versus NWM and NC based on specific spectral and temporal fluorescence characteristics.

4.1 TR-LIFS Features in the Characterization of Brain Tumors versus Normal Brain Tissue

We determined that when the tissue is excited using ultraviolet light (e.g., 337 nm), the emission from two wavelength ranges appeared important for diagnosing gliomas from normal brain tissue: 380 to 400 nm and 440 to 470 nm (the region of main peak emission for NC and LGG and HGG). Striking and distinct fluorescence parameters were observed in LGG when compared with the NC or NWM. One important observation was that LGG shows mainly a single peak of fluorescence emission at 460 nm of wavelength, whereas the NC and NWM demonstrate two fluorescence emission peaks centered at 390 nm and 460 nm. This is interpreted as the presence of a single fluorophore in LGG. This is further reinforced by inspecting the fluorescence lifetimes, which clearly show fast-intensity decay and nearly constant average lifetime values across the fluorescence spectrum. This particular emission with peak at 460 nm and lifetime of around 0.8 to 1.0 ns is attributed to NADH, which demonstrates spectral¹⁰ and temporal^{18,19,21} characteristics as described in previous studies (Table 1).

In contrast to these findings for LGG, normal tissue (i.e., NC and NWM) and HGG demonstrated additional fluorescence emission peak and longer fluorescence lifetimes at 390 nm (1.7 to 1.8 ns). This longer lasting emission at blue-shifted wavelengths when compared to that at red-shifted emission wavelengths suggests that this additional emission peak originates from a distinct fluorophore, other than NADH. While relatively scarce information on the origin of the fluorescence emission of brain tissue at 390 nm on UV (337 nm) has been reported, we identified two possible fluorophores known to emit fluorescence within this wavelength band: Pyridoxamine-5-phosphate (PMP) and glutamate decarboxylase (GAD).²² Both of these fluorophores are metabolically affected in gliomas and are briefly discussed in the following.

Pyridoxine or vitamin B₆ is required by the body to convert carbohydrates to glucose. In addition, the function of pyridoxine is the formation of RNA and DNA, and it plays a role in the removal of the toxic chemical homocysteine. Pyridoxamine phosphate (PMP) along with Pyridoxine phosphate

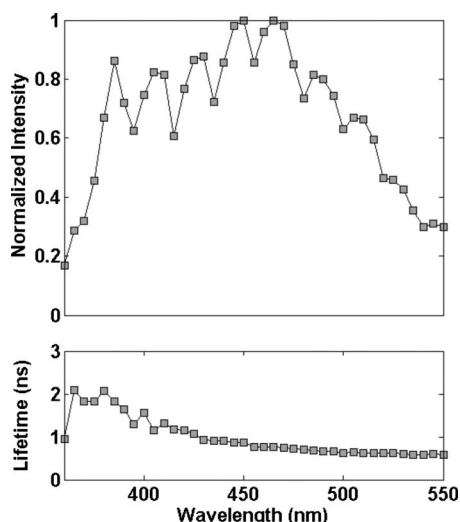


Fig. 5 Example of the fluorescence emission spectrum (intensity values at distinct wavelengths) modulated by the movement of the brain due to breathing. The changes in intensity are due to changes in the excitation-collection during the approximately 30-s data recording (wavelength scanning) time. The figure depicts the variability in fluorescence emission spectrum from NC tissue due to movement of the brain (top). Note: The average lifetime (bottom) from the same tissue samples is not affected by such movements.

(PN) is converted by pyridoxine-5'-phosphate oxidase (PNPO) into pyridoxal phosphate (PLP). PMP fluoresces with peak emission at 390 nm, along with PLP, which fluoresces with emission peak between 315 and 340 nm (Ref. 23). But in hydrated form at neutral pH, it shows similar fluorescence characteristics as PMP. The PLP mechanism is known to be disturbed in cancers.^{24–26} Our TR-LIFS studies of gliomas and normal brain tissue show that there is a decrease/absence of the emission peak at 390 nm of wavelength in glioma when compared with normal cortex tissue. We hypothesize that this may be due to altered metabolism in the PLP mechanism that leads to decrease in the PMP levels in the brain.

The second fluorophore possibly responsible for changes observed at emission peak at 390 nm is glutamate decarboxylase, which is an enzyme essential in the formation of neurotransmitter GABA (γ -amino butyric acid) from amino acid L-glutamate in a single step. Glutamate decarboxylase shows

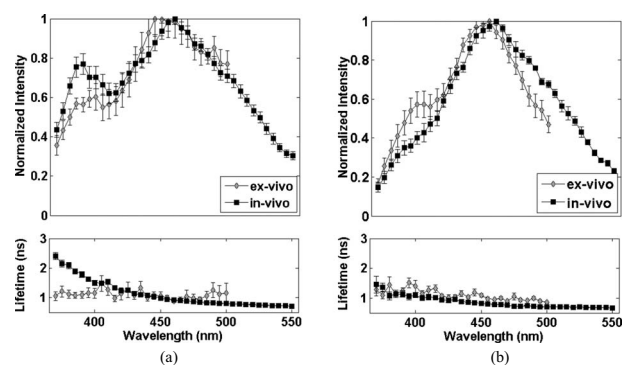


Fig. 6 Group values (mean \pm SE) of a set of spectroscopic parameters derived from *ex vivo* and *in vivo* TR-LIFS measurements: normalized emission spectrum (top) and average lifetime along the emission wavelengths (bottom) of normal cortex, (a) Normal cortex; (b) low-grade glioma.

fluorescence emission maxima at 380 nm of wavelength when excited at 335 nm at neutral pH.²⁷ GABA is a most important inhibitory neurotransmitter found in abundance in the brain.²⁸ The absorption maxima of GAD are 330 nm and 420 nm. GABA_A-benzodiazepine receptors are present in 1/3 of brain, and the $\alpha 1$ subunit of a GABA_A receptor is expressed throughout the brain.²⁹ Most of the GAD is present in the neurons at the synapses. It is known that the activity of this enzyme increases with the differentiation of the neuroblastoma cells. It has been shown that activities of GAD are much lower in the C6 glioblastoma and C1300 neuroblastoma cells than in normal mouse cerebral cortex.³⁰ C6 glioma cells may represent a neuroglial precursor at an early developmental.³¹ Moreover, it is known that malignant glioma cells in rats actively secrete glutamate *in vitro* and that the extracellular levels of glutamate have been shown increased both in and around glioma implants *in vivo*.³² This may suggest an absence of glutamate decarboxylase in its active form in neoplastic tissue.

The ANOVA test performed on various TR-LIFS-derived parameters demonstrated that a small subset of spectral and time-resolved parameters (total: 16) retrieved primarily from a few wavelengths (390, 440, and 460 nm) provide means of discrimination of distinct brain tissue types. This finding is important, as it allows for future design of TR-LIFS devices

Table 1 Summary of fluorescence properties listing all the fluorophores significant in the brain.

Fluorophore	Excitation (nm)	Emission (nm)	Lifetime (ns)	Quantum efficiency	Tissues	References
Pyridoxamine phosphate	330	390	0.11	0.18	Liver, brain, kidney	Ref. 23
Pyridoxal phosphate	330	430	NA	0.03	Liver, brain, kidney	Ref. 23
NADH	340	460	0.4–1.21	0.4–0.69 \pm 0.02	All cells	Refs. 4, 18, and 19
FAD/FMN	370/440	510–520	6–10	NA	Brain, liver	Ref. 23
GAD	335	380	NA	NA	Brain	Ref. 27

that collect fluorescence decay transients at a limited number of spectral bands, as recently reported.³³ In turn, such design will allow for fast data acquisition time (less than 1 s for each point measurement). HGG samples demonstrated a high degree of variability of both fluorescence emission intensity and average lifetime at 390 nm. This variability may be due to a high degree of variation in the genetic as well as metabolic makeup of HGGs. This finding suggests that future studies focused on HGG have to also evaluate the changes in fluorescence parameters as a function of tumor heterogeneity.

While the *in vivo* measurements of fluorescence intensity data are often affected by various factors such as the presence of endogenous absorbers (e.g., blood hemoglobin), variation in fiber-optic probe excitation collection-collection geometry (e.g., moving artifacts due to arterial pulsation or breathing) and photobleaching, we determined that the use of time-resolved (lifetime) information has the potential to account for factors that nonlinearly affect the fluorescence measurement. Figure 5, for example, demonstrates that while in some cases the emission spectrum was significantly altered by breathing artifacts and blood absorption, the average fluorescence lifetime is virtually unaffected. This underscores the importance of using fluorescence decay information as an additional means for tissue discrimination.

4.2 Ex Vivo versus In Vivo TR-LIFS Measurements

Current results demonstrate that the brain tumor fluorescence signatures obtained *in vivo* (in patients undergoing brain tumor surgery) are distinct from those we previously reported for *ex vivo* measurements (brain tumor specimens).^{6,11,12,34} When the fluorescence emission from the *ex vivo* NC tissue was compared with the *in vivo* samples, we noticed that the *ex vivo* samples show a single peak of emission. This suggests that the additional fluorophore emitting at the 390-nm wavelength band is absent in the *ex vivo* samples. The peak emission of NADH also appeared blue-shifted to 440 nm. The difference in the emission characteristics becomes even more evident when the average lifetime at 390 nm and 460 nm are taken into consideration. While the tissue fluorescence measured in *ex vivo* samples demonstrated a uniform average lifetime value across the emission spectrum, the fluorescence measurements in the *in vivo* samples showed a decrease (approximate 2.0 ns at 390 nm versus 1.0 ns at 460 nm) of lifetime values as a function of emission wavelength. The emission spectrum of *ex vivo* NWM showed similar trends (two distinct emission peaks at 390 nm and 460 nm) to the *in vivo* samples. However, the lifetime information at these peaks was found to have slightly longer lifetime at 460 nm in *ex vivo* tissue (~1.8 ns) when compared with the *in vivo* samples (~1 ns). The lifetime at 390 nm is similar in both *ex vivo* and *in vivo* samples of normal white matter (~2.0 ns). LGG fluorescence emission (Fig. 6) in both *ex vivo* and *in vivo* tissue is characterized by a single peak at 460 nm and a uniform lifetime along the emission wavelengths.

While the exact cause of differences in the brain tissue fluorescence emission *ex vivo* versus *in vivo* is still to be determined, we hypothesize that such changes are determined by difference in the environment and/or metabolic changes that may occur after tissue excision. These differences, however, are expected to provide additional insight for future

studies targeted at understanding the origin of fluorescence emission from brain tissue.

5 Conclusion

This study has demonstrated for the first time the ability of a time-resolved fluorescence spectroscopy technique to characterize *in vivo* the biochemical features of primary brain tumors that are clinically relevant. Although this is a pilot study conducted on a small number of patients, we have shown that normal brain tissue (NC, NWM) and LGG are well-characterized by distinct fluorescence emission features. Fluorescence temporal features including average lifetime and Laguerre coefficients derived from three spectral emission bands centered at 390, 440, and 460 nm can be used to distinguish LGG from normal brain tissue. Thus, future optimization of TR-LIFS data acquisition at these predefined wavelength bands³³ centered around these wavelengths combined with the fast analysis of the fluorescence intensity decay facilitated by the Laguerre expansion of kernels deconvolution approach,^{16,17} will enable near-real time (less than 1 s) tissue diagnosis. We also determined that while fluorescence of LGG is distinct and can be used to clearly delineate from normal tissue, HGG fluorescence characteristics have a large variability, which appears to be correlated with heterogeneous composition of high-grade glioma, a factor that is not taken into account in the conventional gross histopathological diagnosis or classification of the brain biopsy sample. We also observed differences in the emission characteristics between the *ex vivo* and *in vivo* tissues that indicate a possible change in the biochemical composition of tissue after excision. This finding suggests that studies conducted in brain tissue specimens cannot be fully translated to the *in vivo* situation. In turn, this emphasizes the need for further validation of fluorescence-based diagnostic devices directly *in vivo* in a large number of patients and development of optimized TR-LIFS devices that allow for clinical investigations. Current study has provided the base of knowledge that will enable further development of such TR-LIFS devices.

Acknowledgments

This work was supported in part by the Whitaker Foundation (RG-01-0346, PI: L. Marcu) and the Maxine-Dunitz Neurosurgical Institute at Cedars-Sinai Medical Center and by the WISE Fund at the University of Southern California.

References

1. A. A. Brandes, A. Tosoni, E. Franceschi, M. Reni, G. Gatta, and C. Vecht, "Glioblastoma in adults," *Crit. Rev. Oncol. Hematol.* **67**(2), 139–152 (2008).
2. J. T. Fazekas, "Treatment of grades I and II brain astrocytomas. The role of radiotherapy," *Int. J. Radiat. Oncol., Biol., Phys.* **2**(7–8), 661–666 (1977).
3. S. A. Leibel, G. E. Sheline, W. M. Wara, E. B. Boldrey, and S. L. Nielsen, "The role of radiation therapy in the treatment of astrocytomas," *Cancer* **35**(6), 1551–1557 (1975).
4. Y. G. Chung, J. A. Schwartz, C. M. Gardner, R. E. Sawaya, and S. L. Jacques, "Diagnostic potential of laser-induced autofluorescence emission in brain tissue," *J. Korean Med. Sci.* **12**(2), 135–142 (1997).
5. A. C. Croce, S. Fiorani, D. Locatelli, R. Nano, M. Ceroni, F. Tancioni, E. Giombelli, E. Benericetti, and G. Bottiroli, "Diagnostic potential of autofluorescence for an assisted intraoperative delineation of glioblastoma resection margins," *Photochem. Photobiol.* **77**(3), 309–318 (2003).

6. L. Marcu, J. A. Jo, P. V. Butte, W. H. Yong, B. K. Pikul, K. L. Black, and R. C. Thompson, "Fluorescence lifetime spectroscopy of glioblastoma multiforme," *Photochem. Photobiol.* **80**, 98–103 (2004).
7. W. S. Poon, K. T. Schomacker, T. F. Deutsch, and R. L. Martuza, "Laser-induced fluorescence: experimental intraoperative delineation of tumor resection margins," *J. Neurosurg.* **76**(4), 679–686 (1992).
8. G. A. Wagnieres, W. M. Star, and B. C. Wilson, "In vivo fluorescence spectroscopy and imaging for oncological applications," *Photochem. Photobiol.* **68**(5), 603–632 (1998).
9. W. C. Lin, S. A. Toms, M. Johnson, E. D. Jansen, and A. Mahadevan-Jansen, "In vivo brain tumor demarcation using optical spectroscopy," *Photochem. Photobiol.* **73**(4), 396–402 (2001).
10. W. C. Lin, S. A. Toms, M. Motamedi, E. D. Jansen, and A. Mahadevan-Jansen, "Brain tumor demarcation using optical spectroscopy: an in vitro study," *J. Biomed. Opt.* **5**(2), 214–220 (2000).
11. P. V. Butte, B. K. Pikul, A. Hever, W. H. Yong, K. L. Black, and L. Marcu, "Diagnosis of meningioma by time-resolved fluorescence spectroscopy," *J. Biomed. Opt.* **10**(6), 064026 (2005).
12. W. H. Yong, P. V. Butte, B. K. Pikul, J. A. Jo, Q. Fang, T. Papaioannou, K. Black, and L. Marcu, "Distinction of brain tissue, low grade, and high grade glioma with time-resolved fluorescence spectroscopy," *Front. Biosci.* **11**, 1255–1263 (2006).
13. Q. Fang, T. Papaioannou, J. A. Jo, K. Vaitha, and L. Marcu, "Time-domain laser-induced fluorescence spectroscopy apparatus for clinical diagnostics," *Rev. Sci. Instrum.* **75**(1), 151–162 (2004).
14. T. Papaioannou, N. Preyer, Q. Fang, M. Carmohan, R. Ross, A. Brightwell, G. Cottone, L. Jones, and L. Marcu, "Effects of fiberoptic probe design and probe-to-target distance on diffuse reflectance measurements of turbid media: an experimental and computational study at 337 nm," *Appl. Opt.* **43**(14), 2846–2860 (2004).
15. D. N. Louis, H. Ohgaki, O. D. Wiestler, W. K. Cavenee, P. C. Burger, A. Jouvet, B. W. Scheithauer, and P. Kleihues, "The 2007 WHO classification of tumors of the central nervous system," *Acta Neuropathol.* **114**(2), 97–109 (2007).
16. J. A. Jo, Q. Fang, T. Papaioannou, and L. Marcu, "Fast model-free deconvolution of fluorescence decay for analysis of biological systems," *J. Biomed. Opt.* **9**(4), 743–752 (2007).
17. J. A. Jo, Q. Fang, T. Papaioannou, J. H. Qiao, M. C. Fishbein, B. Beseth, A. H. Dorafshar, T. Reil, D. Baker, J. Freischlag, and L. Marcu, "Application of the Laguerre deconvolution method for time-resolved fluorescence spectroscopy to the characterization of atherosclerotic plaques," in *Proc. 27th Ann. Conf. of IEEE Engineering in Medicine and Biology Society*, pp. 6559–6562, IEEE, Piscataway, NJ (2005).
18. A. Pradhan, P. Pal, G. Durocher, L. Villeneuve, A. Balassy, F. Babai, L. Gaboury, and L. Blanchard, "Steady state and time-resolved fluorescence properties of metastatic and non-metastatic malignant cells from different species," *J. Photochem. Photobiol., B* **31**(3), 101–112 (1995).
19. K. C. Reinert, R. L. Dunbar, W. Gao, G. Chen, and T. J. Ebner, "Flavoprotein autofluorescence imaging of neuronal activation in the cerebellar cortex in vivo," *J. Neurophysiol.* **92**(1), 199–211 (2004).
20. D. M. Jameson, V. Thomas, and D. M. Zhou, "Time-resolved fluorescence studies on NADH bound to mitochondrial malate dehydrogenase," *Biochim. Biophys. Acta* **994**(2), 187–190 (1989).
21. K. Konig, M. W. Berns, and B. J. Tromberg, "Time-resolved and steady-state fluorescence measurements of beta-nicotinamide adenine dinucleotide-alcohol dehydrogenase complex during UVA exposure," *J. Photochem. Photobiol., B* **37**(1–2), 91–95 (1997).
22. R. Shukuya and G. W. Schwert, "Glutamic acid decarboxylase. II. The spectrum of the enzyme," *J. Biol. Chem.* **235**, 1653–1657 (1960).
23. W. R. Zipfel, R. M. Williams, R. Christie, A. Y. Nikitin, B. T. Hyman, and W. W. Webb, "Live tissue intrinsic emission microscopy using multiphoton-excited native fluorescence and second harmonic generation," *Proc. Natl. Acad. Sci. U.S.A.* **100**(12), 7075–7080 (2003).
24. E. O. Ngo, G. R. LePage, J. W. Thanassi, N. Meisler, and L. M. Nutter, "Absence of pyridoxine-5'-phosphate oxidase (PNPO) activity in neoplastic cells: isolation, characterization, and expression of PNPO cDNA," *Biochemistry* **37**(21), 7741–7748 (1998).
25. S. K. Sharma and K. Dakshinamurti, "Determination of vitamin B6 vitamers and pyridoxic acid in biological samples," *J. Chromatogr.* **578**(1), 45–51 (1992).
26. K. O. Honikel and N. B. Madsen, "Comparison of the absorbance spectra and fluorescence behavior of phosphorylase b with that of model pyridoxal phosphate derivatives in various solvents," *J. Biol. Chem.* **247**(4), 1057–1064 (1972).
27. S. Udenfriend, *Fluorescence Assay in Biology and Medicine*, Vols. I and II, Academic Press, New York (1969).
28. P. Flace, V. Benagiano, L. Lorusso, F. Girolamo, A. Rizzi, D. Virgintino, L. Roncali, and G. Ambrosi, "Glutamic acid decarboxylase immunoreactive large neuron types in the granular layer of the human cerebellar cortex," *Anat. Embryol. (Berl)* **208**(1), 55–64 (2004).
29. H. K. Wolf, R. Buslei, I. Blumcke, O. D. Wiestler, and T. Pietsch, "Neural antigens in oligodendrogliomas and dysembryoplastic neuroepithelial tumors," *Acta Neuropathol.* **94**(5), 436–443 (1997).
30. L. Ossola, M. Maitre, J. M. Blindermann, and P. Mandel, "Enzymes of GABA metabolism in tissue culture," *Adv. Exp. Med. Biol.* **123**, 139–157 (1979).
31. J. Segovia, G. M. Lawless, N. J. Tillakaratne, M. Brenner, and A. J. Tobin, "Cyclic AMP decreases the expression of a neuronal marker (GAD67) and increases the expression of an astroglial marker (GFAP) in C6 cells," *J. Neurochem.* **63**(4), 1218–1225 (1994).
32. T. Takano, J. H. Lin, G. Arcuino, Q. Gao, J. Yang, and M. Nedergaard, "Glutamate release promotes growth of malignant gliomas," *Nat. Med.* **7**(9), 1010–1015 (2001).
33. Y. Sun, R. Liu, D. S. Elson, C. W. Hollars, J. A. Jo, J. Park, and L. Marcu, "Simultaneous time- and wavelength-resolved fluorescence spectroscopy for near real-time tissue diagnosis," *Opt. Lett.* **33**(6), 630–632 (2008).
34. L. Marcu, M. C. Fishbein, J. M. Maarek, and W. S. Grundfest, "Discrimination of human coronary artery atherosclerotic lipid-rich lesions by time-resolved laser-induced fluorescence spectroscopy," *Arterioscler., Thromb., Vasc. Biol.* **21**(7), 1244–1250 (2001).